Supporting Information

Cross-linked copolymer derived nitrogen-doped hierarchical porous carbon with high-performance lithium storage capability

Rui Luo,[a] ‡ Zhengwei Wan,[c] ‡ Peng Mei,*[ab] Zhengjiao Xie,[a] Dean Shi,[b] and Yingkui Yang*[ac]

[a] Key Laboratory of Catalysis and Energy Materials Chemistry of Ministry of Education & Hubei Key Laboratory of Catalysis and Materials Science, South-Central Minzu University, Wuhan 430074, China
E-mail: meipeng@scuec.edu.cn

[b] Ministry-of-Education Key Laboratory for Green Preparation and Application of Functional Materials, Hubei University, Wuhan 430074, China

[c] Hubei Engineering Technology Research Centre of Energy Polymer Materials, School of Chemistry and Materials Science, South-Central Minzu University, Wuhan 430074, China
E-mail: ykyang@mail.scuec.edu.cn

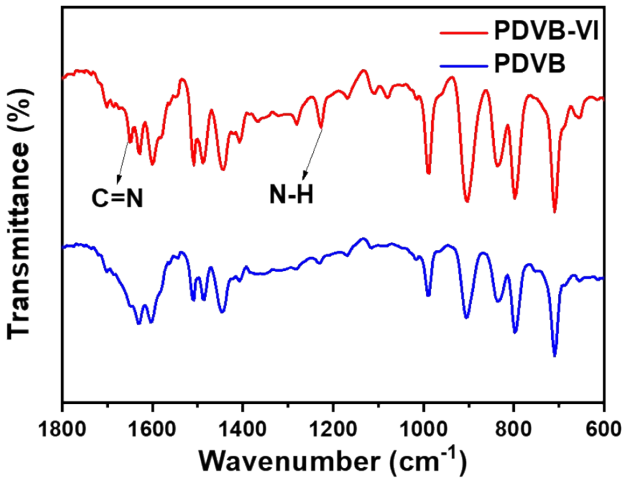

Fig. S1 FTIR spectra of PDVB-VI and PDVB.

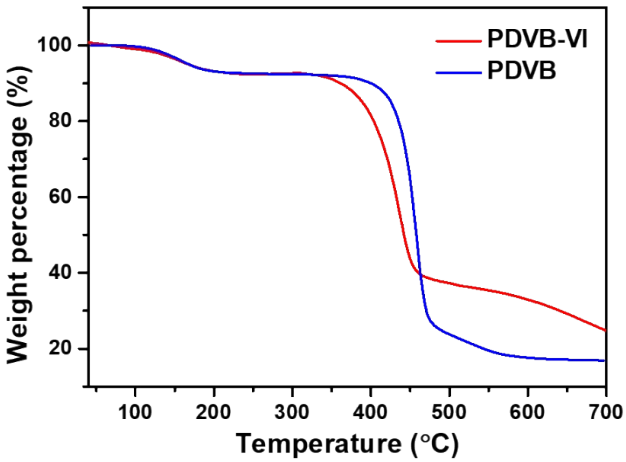

Fig. S2 TG curves of PDVB-VI and PDVB under N_2 flow.

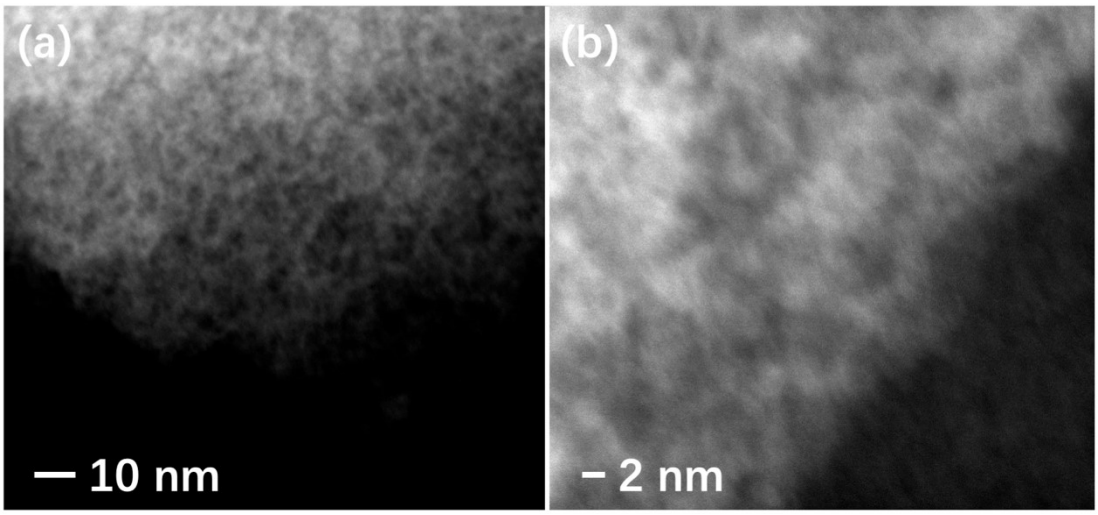

Fig. S3 (a) STEM and (b) HR-TEM images of N-HPC.

Table S1. Detailed pore structure parameters of N-HPC and HPC

Sample	S_{BET} (m^2g^{-1})	V_{total} (cm^3g^{-1})	V_{micro} (cm^3g^{-1})	V_{micro}/V_{total}
N-HPC	1685 m^2/g	1.10147	0.426443	38.72%
HPC	815 m^2/g	0.792166	0.239944	30.29%

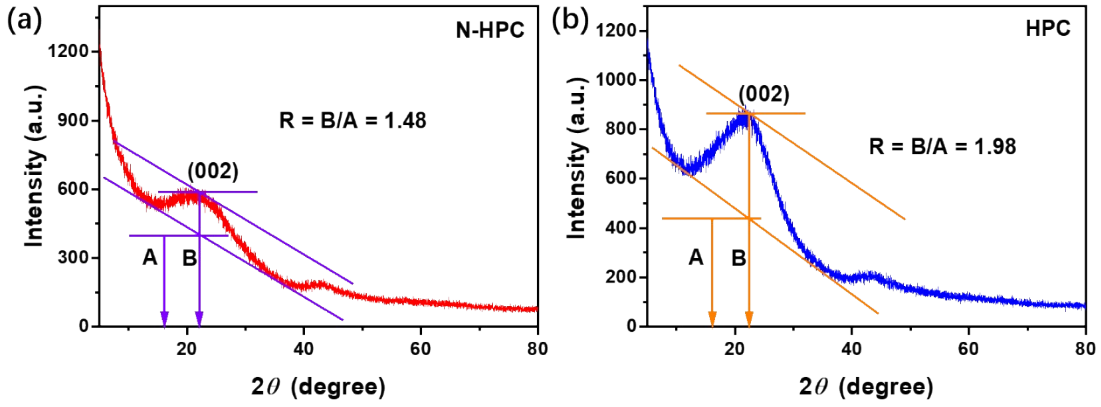

Fig. S4 Schematic representation of R used to empirically estimate the fraction of single layers present in (a) N-HPC and (b) HPC.

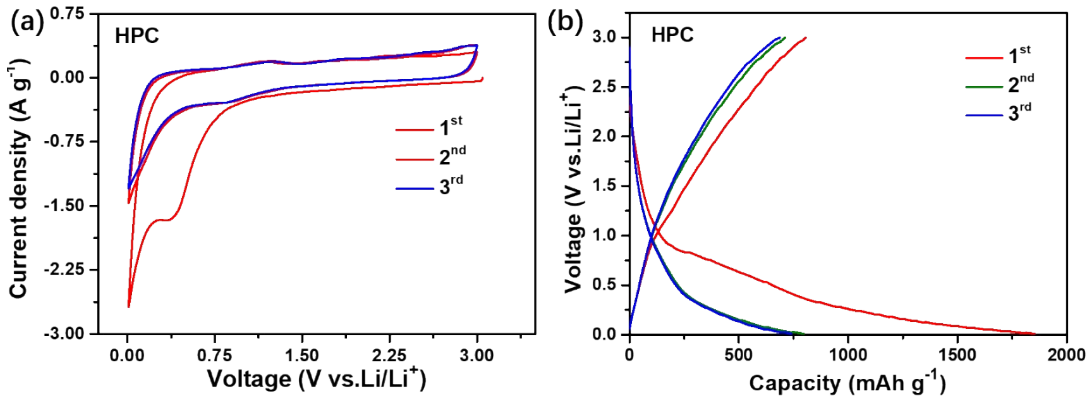

Fig. S5 (a) First three CV curves at 0.5 mV s^{-1} and (b) charge/discharge curves at 0.1 A g^{-1} of N-HPC.

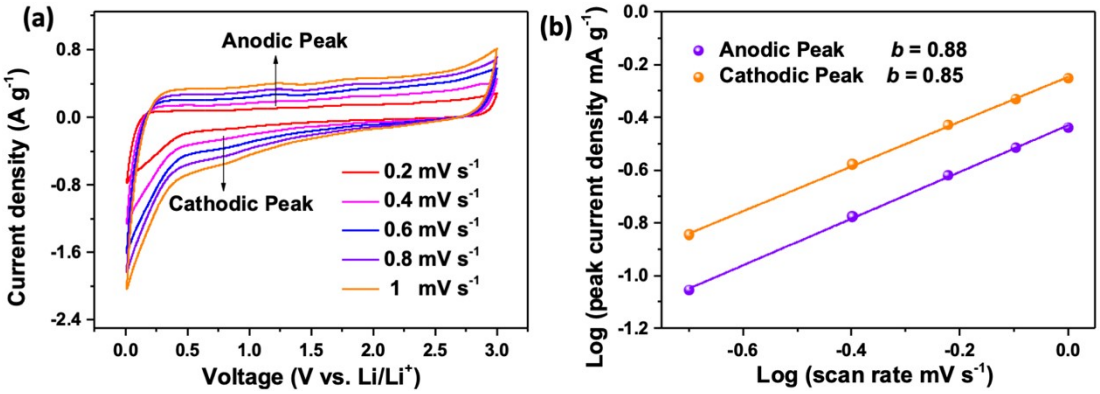

Fig. S6 Kinetics analysis of the electrochemical behavior of N-HPC: (a) CV curves at various scan rates and (b) linear relationship of log(*i*) and log(*v*).

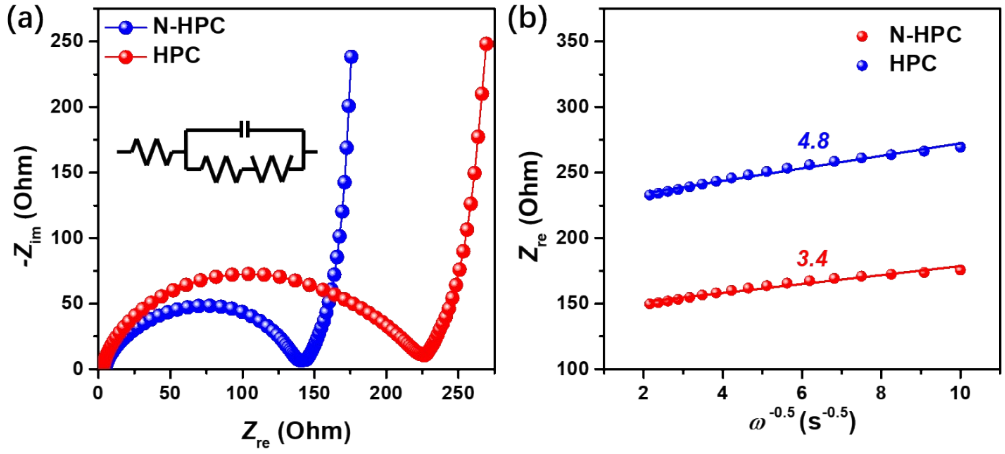

Fig. S7 (a) Nyquist plots of N-HPC and HPC; (b) the relationship between the real part of the impedance (Z_{re}) and the reciprocal of the square root of frequency ($\omega^{-1/2}$) in the low-frequency Warburg range for N-HPC and HPC.

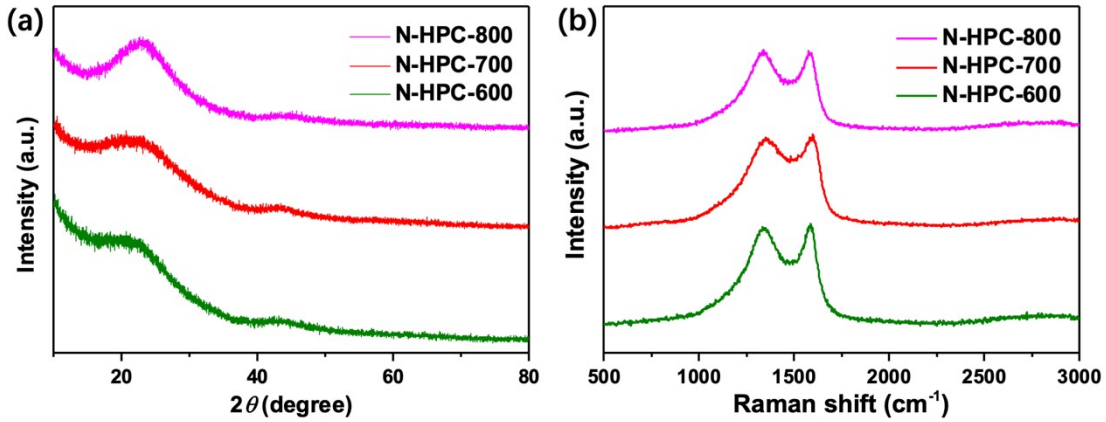

Fig. S8 (a) XRD patterns and (b) Raman spectra of the N-HPC samples (N-HPC-600, N-HPC-700, N-HPC-800) obtained under different annealing temperatures (600 °C, 700 °C, 800 °C).

Note on Fig. S8

Apart from the control sample HPC, we have carbonized the KOH-impregnated PDVB-VI precursors under different temperatures (600 °C, 700 °C, 800 °C) to conduct additional control experiments, to investigate the effect of annealing temperature on the resultant structural and electrochemical features. The crystallographic textures of the N-HPC samples (N-HPC-600, N-HPC-700, N-HPC-800) have been characterized by XRD. As shown in **Fig. S8a**, two typical diffraction peaks appear at around 23° and 43° for all the samples, representing the (002) and (100) crystal planes of graphitic carbon. Furthermore, the peak shape becomes more distinguishable with increasing the annealing temperature, which is understandable since higher temperature is more favorable for the graphitization process. Raman spectra are further inspected for the N-HPC samples to disclose their carbon structure features. The corresponding I_D/I_G values acquired from **Fig. S8b** are 1.20, 1.36, and 1.11 for N-HPC-600, N-HPC-700, and N-HPC-800, respectively. The variation rule of I_D/I_G is reasonably expected for the N-HPC samples and their defect content is supposed to follow the ordering of N-HPC-600 < N-HPC-800 < N-HPC-700. This result can be elucidated as follows: as the annealing temperature increase from 600 to 700 °C, the continuous decomposition of polymer segments has generated the carbon matrix and further introduced heteroatom

(nitrogen) into the carbon framework, thereby leading to an increased amount of structure defects; when the temperature is elevated to 800 °C, the graphitization process is highly promoted while the volatile heteroatom is less likely to remain in the carbon matrix. Consequently, the structural ordering is improved and the defect content is reduced.

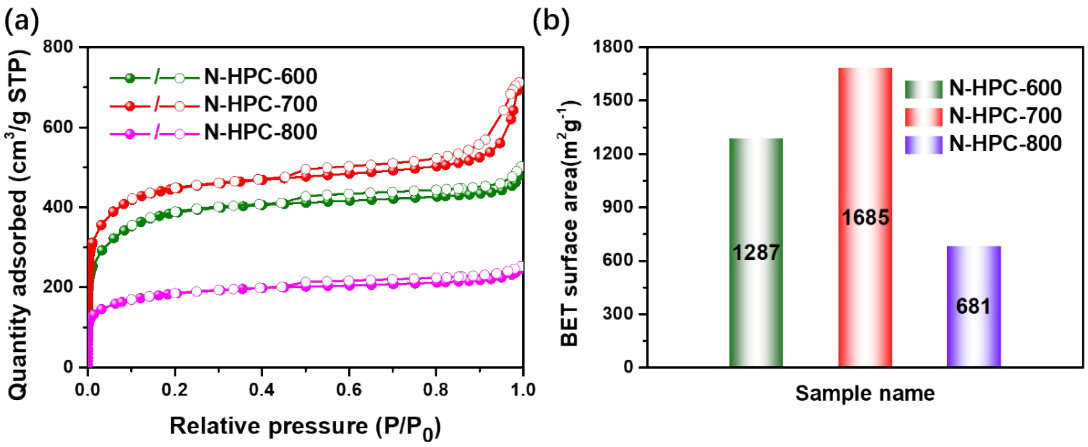

Fig. S9 (a) Nitrogen adsorption-desorption isotherms and (b) corresponding BET surface areas of the N-HPC samples (N-HPC-600, N-HPC-700, N-HPC-800).

Note on Fig. S9

The pore structure of the N-HPC samples has been further inspected by nitrogen adsorption-desorption analysis. As shown in **Fig. S9a**, all the N-HPC samples display the same type isotherms but vary in the quantity of N_2 adsorbed either in total or in the low-pressure region. Notably, N-HPC-700 shows the most remarkable N_2 adsorption in the low pressures, implying that it should contain the largest amount of micropores. As far as we know, micropores play the dominant role in enlarging the materials' specific surface area. After calculations by the BET method, the specific surface areas are 1287, 1685, and 681 m^2 g^{-1} for N-HPC-600, N-HPC-700, and N-HPC-800, respectively (**Fig. S9b**). Such change trend might be explained as follows: with increasing the annealing temperature from 600 °C to 700 °C, the carbonization process of the polymer precursor is favorably facilitated and more micropores are generated upon further decomposition of the organic moieties. Nevertheless, as the annealing temperature further increases, the generated micropores might grow into larger-sized pores by self-aggrandizement or mergence. As a result, the specific surface area would decrease due to the loss of micropores. Therefore, the optimal pore structure of N-HPC-700 should allow itself the best electrochemical performance when used as LIBs anode.

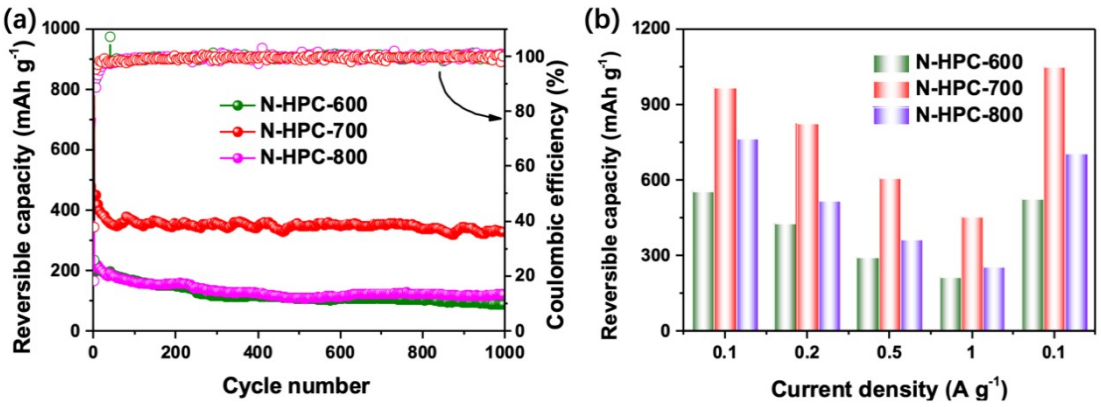

Fig. S10 (a) Cycling performance at 2 A g^{-1} and (b) average reversible capacities at various current densities for the N-HPC samples (N-HPC-600, N-HPC-700, N-HPC-800).

Note on Fig. S10

The electrochemical properties of the N-HPC samples as anode for LIBs have been evaluated by galvanostatic charge-discharge measurements. The service life and fast charging-discharging properties of the batteries have attracted close attention in the present and future society. **Fig. S10a** compares the cycling performance of the N-HPC samples at a large current density of 2 A g^{-1}. As expected, N-HPC-700 delivers considerably high initial reversible capacity of 450.5 mAh g^{-1}, which is much higher than the other two (192.9 and 214.7 mAh g^{-1} for N-HPC-600 and N-HPC-800, respectively). After repeatedly charged and discharged for 1000 times, N-HPC-700 still retains an appreciable reversible capacity of 331.6 mAh g^{-1}, which is about 3 ~ 4 times higher than that of N-HPC-600 (86.2 mAh g^{-1}) and N-HPC-800 (120.6 mAh g^{-1}), indicating the superior long-term cyclic stability of N-HPC-700 among the three. **Fig. S10b** summarizes the average reversible capacities of the N-HPC samples at different current densities from 0.1 A g^{-1} to 1 A g^{-1}. As the current density increases stepwise, the reversible capacity of the N-HPC-700 decreases slowly and steadily from 967.7 mAh g^{-1} at 0.1 A g^{-1}, to 824.9, 606.6, and 451.6 mAh g^{-1} at 0.2, 0.5, 1 A g^{-1}, respectively, which easily outperforms the control samples of N-HPC-600 and N-HPC-800 at each rate. Specifically, the average capacities of N-HPC-600 and N-HPC-800 are 555.8 and

763.4 mAh g^{-1} at 0.1 A g^{-1}, 425.4 and 516.8 mAh g^{-1} at 0.2 A g^{-1}, 291.3 and 362.6 mAh g^{-1} at 0.5 A g^{-1}, 213.1 and 254.8 mAh g^{-1} at 1.0 A g^{-1}. Moreover, when the current density returns to 0.1 A g^{-1}, the capacity of N-HPC-700 even exceeds its initial value (1047.6 mAh g^{-1}), while the other two fail to fully recover their capacities. Obviously, N-HPC-700 exhibits the most remarkable rate capability amongst all the N-HPC samples. In short, N-HPC-700 has demonstrated the best overall electrochemical performance as LIBs anode, which should be attributed to its optimized porous structure with large specific surface area and high defect content. Therefore, 700 °C is proved to be the optimal annealing temperature in our case.